International Journal of Solids and Structures 50 (2013) 3717–3722

Contents lists available at ScienceDirect

International Journal of Solids and Structures

journal homepage: www.elsevier.com/locate/ijsolstr

Buckling-induced dislocation emission in thin films on substrates

Antoine Ruffini *, Julien Durinck, Jérôme Colin, Christophe Coupeau, Jean Grilhé

Institut P', CNRS-Université de Poitiers-ENSMA, Département Physique et Mécanique des Matériaux, SP2MI-Téléport 2, F86962 Futuroscope-Chasseneuil cedex, France

ARTICLE INFO

Article history:
Received 4 August 2012
Received in revised form 29 March 2013
Available online 27 July 2013

Keywords:
Thin-films
Dislocations
Misfit
Buckling
Atomistic simulations
Analytical modelling

ABSTRACT

Atomistic simulations of the evolution of a strained thin film on a substrate has been reported and the formation of dislocations has been observed in the film/substrate interface after the film has buckled. In the framework of the linear elasticity theory, an analytical model has been developed to explain the buckle effect on the formation of the dislocations. A stability diagram with respect to the buckling and dislocation emission phenomena is finally presented for the film as a function of the uniaxial strain and the Burgers vector.

1. Introduction

Low-dimensional structures such as thin films on substrates and coatings have been intensively studied in the past few years in a number of engineering fields ranging from electronics to optics. In the framework of materials science and solid mechanics, the stresses resulting from the techniques of deposition and/or the physical properties of the materials involved in the low-dimensional structures (such as the dilatation coefficients, the shear modulii or the lattice parameters) have been found to strongly modify their mechanical properties, stability and ageing. Different relaxation mechanisms have been thus observed to release the stored elastic energy. For example, one can cite the cracking of the films (Hu and Evans, 1989; Zhao et al., 2002) or the morphological evolution of their surface (Gao, 1994; Yang, 2006) which may lead to the deterioration of the film/substrate structures and the loss of their functional properties.

The interfaces between the films and their substrate have been also identified as preferential regions where the relaxation mechanisms may occur. The formation of misfit dislocations is one of them in the case where a lattice mismatch at the interfaces generates misfit strains in both materials (Frank and Van Der Merwe, 1949). In this case, a critical thickness can be defined for the film below which misfit dislocations can not be observed. The formation of such misfit dislocations has been investigated from surface steps, interfacial defects or from pre-existing threading dislocations (Godet et al., 2006; Henager and Hoagland, 2004; Spearot et al., 2007; Matthews and Blakeslee, 1974; Braun et al., 2002; Cantu et al., 2005), and their propagation in the different layers has been analysed (Grilhé, 1993; Youssef et al., 2008; Shao and Medyanik, 2010).

The delamination of the interfaces and the thin film buckling (Gioia et al., 1997; Freund and Suresh, 2003) may also release the elastic energy of the strained structures. In the framework of the Föppl-von Kármán (FvK) theory of thin plates (Hutchinson and Suo, 1992), several buckling structures have been characterized such as circular blisters (Faulhaber et al., 2006; Kuznetsov et al., 2012), telephone cord (Cordill et al., 2007; Lee et al., 2005) or straight-sided buckles (SSB) (Audoly, 1999; Parry et al., 2004). Recently, the plasticity of the buckles has been considered (Cordill et al., 2005; Durinck et al., 2008; Ruffini et al., 2012) and the formation of dislocations from the top side of the buckles or the folding of the buckling structures due to grains boundaries have been studied (Durinck et al., 2010; Colin et al., 2007). In this paper, the plasticity localized at the coherent dislocation-free interface of the adherent part of a strained thin film on a substrate is studied theoretically after buckling of the delaminated part of the film and the formation of misfit dislocations in the film/substrate interface near the buckle has been characterized. To do so, atomistic simulations of the buckling of a thin film of molybdenum (Mo) on a stiff substrate of tungsten (W) are first presented and the formation of interfacial dislocations at the edges of a straight-sided buckle is reported. An analytical model is then developed to analyze the buckle effect on the formation of the misfit dislocations.

2. Atomistic simulations of the buckling

An interface between a Mo film and a W substrate is constructed by joining together the (110) planes of the both body-centered cubic (bcc) single crystals. Because the lattice parameters of

* Corresponding author. Tel.: +33 549 49 68 30; fax: +33 549 49 66 92.
E-mail address: antoine.ruffini@univ-poitiers.fr (A. Ruffini).

0020-7683/$ - see front matter © 2013 Elsevier Ltd. All rights reserved.
http://dx.doi.org/10.1016/j.ijsolstr.2013.07.015

both materials are similar, a coherent interface has been chosen for this study. This ensures that the starting interface is free of misfit dislocations. The (Ox) axis of the system is aligned along the $\left[1\bar{1}1\right]_{bcc}$ direction and the (Oz) axis along the $\left[1\bar{1}2\right]_{bcc}$ direction. The (Oy) axis is then along the $[110]_{bcc}$ direction perpendicular to the interface according to Fig. 1. In such an orientation, the dimensions of the unit cell are given by $a_x^{Mo} = a_{Mo} \times \sqrt{3}/2 = 0.273$ nm and $a_x^W = a_W \times \sqrt{3}/2 = 0.274$ nm along the (Ox) axis and $a_z^{Mo} = a_{Mo} \times \sqrt{6} = 0.771$ nm and $a_z^W = a_W \times \sqrt{6} = 0.775$ nm along the (Oz) axis. Taking the unstrained configuration of the substrate of tungsten as the reference strain, the epitaxial strain of the coherent interface is equal to:

$$\varepsilon_{ep} = \frac{a_W - a_{Mo}}{a_{Mo}} = 0.57\%. \tag{1}$$

Four bicrystals with different sizes are compared in this work. The thickness h of the Mo film takes the values 3.1, 4.0, 6.3 and 12.6 nm corresponding respectively to the stacking of 15, 19, 29 and 57 Mo atomic monolayers spaced by about 0.225 nm along the (Oy) axis. The length L_x along the (Ox) axis is chosen to be successively 76.8, 98.7, 153.5 and 307.0 nm (280, 360, 560 and 1120 unit cells respectively) such that the ratio h/L_x remains constant for the four bicrystals. Periodic boundary conditions are applied along the (Ox) and (Oz) directions. The free surfaces are considered along the (Oy) axis perpendicular to the interface. The length along the (Oz) axis corresponds to one unit cell such that the deformation does not vary with z. The simulations have been thus carried out in a two dimensional system. The thickness of the W substrate is identical for the four bicrystals and equal to 4.5 nm corresponding to 20 W atomic monolayers. A vertical distance of 0.200 nm is initially introduced between the film and the substrate.

EAM (Embedded-Atom Method) potentials (Daw and Baskes, 1984) determined by Zhou et al. (2001) are used for Mo-Mo and W-W interactions, and the Johnson's alloy model is applied in turn to generate the Mo-W potential from the single atom potentials (Johnson, 1989). Using the LAMMPS code (Plimpton, 1995), a conjugate gradient minimization procedure is performed to relax the atomic positions keeping L_x and L_z constant.

Interactions between the Mo and W atoms are turned off in the parts of the bicrystal located in $x \in [0, L_x/2]$ and $z \in [0, L_z]$ which corresponds respectively to the regions 1 and 2 in Fig. 1. This procedure leads to the creation of a delaminated zone extending over a width $2B_0 = L_x/2$ along the (Ox) axis.

A compressive strain ε_a is applied step-by-step to the bicrystal along the (Ox) axis with a unit step $\delta\varepsilon_{xx} = -0.025\%$. At each step a conjugate gradient relaxation is performed. At the ith step, the strain in the film is thus given by $\varepsilon_i \approx \varepsilon_{ep} + \varepsilon_a$, where $\varepsilon_a = i\delta\varepsilon_{xx}$. In order to prevent the buckling of the substrate, the W atoms located at the free surface of the substrate are not allowed to move along the (Oy) axis. Since the simulations give equivalent qualitative results for the four values of the film thickness, the system evolution is only presented for one thickness $h = 3.1$ nm of the film.

The buckling of the film into a straight-sided buckle is observed in the range $\varepsilon_i \in [-1.94\%; -5.36\%]$ as it is shown in Fig. 2(a) by the increase of the maximum deflection of the film with respect to the strain ε_i. For $\varepsilon_i < -5.36\%$, the fracture of the Mo film occurs but this point is not investigated here. As it has already been demonstrated in a previous work (Ruffini et al., 2012), a sliding of the film over the substrate occurs at the base of the SSB displacing atoms, from the adherent part to the free buckled part. The relative displacements Δ_0 and Δ_{2B} of the atoms originally located in the middle of the film ($y = h/2$) at $x = 0$ and $x = 2B$ respectively (see Fig. 1) with respect to the position of the decohesion fronts are extracted from the simulation. The average sliding of the film is then calculated by $\Delta = \frac{\Delta_0 - \Delta_{2B}}{2}$ and has been plotted in Fig. 2(b) as a function of the strain. It is seen that two discrete glide events "S1" and "S2" occur during the buckling and are correlated with two sudden jumps on the curve $\delta = f(\varepsilon_i)$. It has already been shown that the maximum buckle deflection δ depends on the average slip displacement Δ (Ruffini et al., 2012) as:

$$\delta = \frac{4B}{\pi}\sqrt{\varepsilon_c - \left(\varepsilon_i - \frac{\Delta}{B}\right)}, \tag{2}$$

where $2B = (1 + \varepsilon_a)2B_0$ and ε_c is the critical compressive strain for the buckling to occur (Hutchinson and Suo, 1992):

$$\varepsilon_c = -\frac{\pi^2}{12}\left(\frac{h}{B}\right)^2. \tag{3}$$

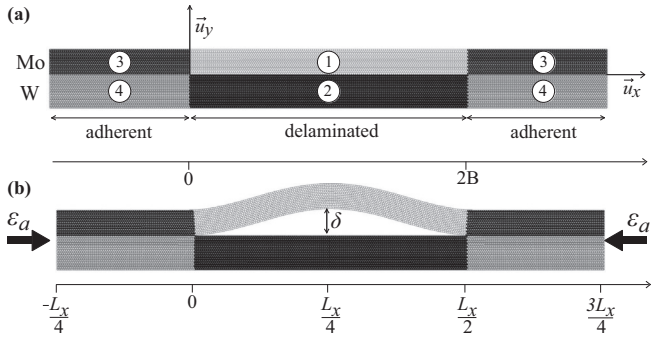

Fig. 1. Front view of the snapshot of the bicrystal (a) before and (b) after the buckling. The left crack-tip of the straight-sided buckle is taken as the origin of the coordinate system.

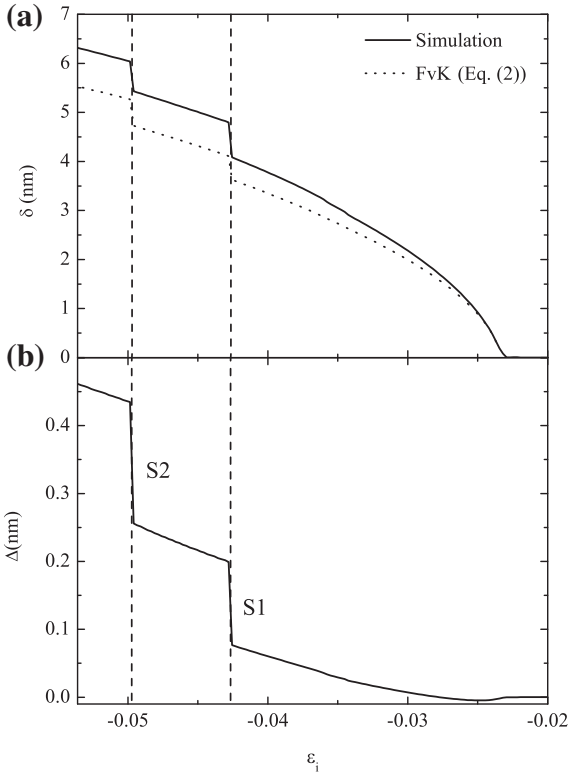

Fig. 2. (a) Maximal deflection δ of the buckle versus ε_i. (b) Average slip displacement Δ versus ε_i. The maximum deflection jumps are correlated to the sliding events "S1" and "S2" according to Eq. (2).

On the atomic scale, these glide events are related to the nucleation and glide of misfit dislocations at the film/substrate interface. Because of the axial symmetry of the SSB, the following analysis is only focused on the decohesion front located at $x = 0$.

Three configurations are extracted from the simulation at $\varepsilon_i = -1.94\%$, -4.28% and -4.98%, before and after each glide event "S1" and "S2". Figs. 3 show the corresponding snapshots where only the atoms in a non-bcc environment have been represented, which allows for the location of the free surfaces and defects like dislocations. The components S_x and S_z of the disregistry vector (Demkowicz et al., 2008) are also plotted in Figs. 3. They stand for the edge and screw components of the Burgers vector of the misfit dislocations.

In Fig. 3(a), the interface remains coherent until an edge dislocation with a Burgers vector $\frac{1}{2}\left[1\bar{1}1\right]_W$ is nucleated at about $\varepsilon_i = -4.28\%$. In Fig. 3(b), the equilibrium position of the dislocation from the buckle edge shifts from $x = -3.4 \pm 0.25$ nm to $x = -4.4 \pm 0.25$ nm at $\varepsilon_i = -4.98\%$, as the compressive strain increases. Another edge dislocation with the same Burgers vector is then nucleated and remains located at about $x \approx -2.8$ nm until the fracture of the thin film occurs at $\varepsilon_i = -5.36\%$. The first dislocation moves then further away from the buckle edge between the second one and the boundary of the simulation box. Because of the use of periodic boundary conditions along the (Ox) axis, the two dislocations nucleated at the left and right buckle edges interact when they approach the boundaries of the simulation box, leading to a repulsive configuration. However, it has been checked (but not presented) that the values of the critical strain for the nucleation of the first dislocations and their equilibrium positions are not modified when larger simulation box lengths along (Ox) are considered. It is thus believed that no artifact due to the periodic boundary conditions along (Ox) takes place in the simulations.

In the three other simulations corresponding to different film thickness h, the results are similar with a nucleation of the first dislocation occurring at $\varepsilon_i = -3.95\%$, -3.50% and -2.94% (for $h = 4.0$, 6.3 and 12.6 nm respectively), the equilibrium distance from the buckle edge being of the order of the film thickness.

3. Modeling of the buckle effect

According to the results of the simulations presented in the previous section, an edge dislocation (d) of Burgers vector $\vec{b} = -b\vec{u_x}$ is introduced into the film/substrate interface at a distance $x < 0$ from the buckle (see Fig. 4). In order to get some insight into the buckle effect on the formation of the dislocation, the following assumptions have been made to determine the force applied on this dislocation which results from the shear stress component. It is supposed that the elastic effects of the buckle can be determined by considering a distribution of line forces onto the vertical free surface of an idealized structure composed of the planar and adherent part of the film of thickness h embedded in a semi-infinite matrix (see Fig. 4). Indeed, since the stress effect of the buckle in the film/substrate interface is only required near the edge of the buckle, i.e. for $|x| < h$ and $y = 0$, the effect of the horizontal free surface of the film ($y = h$) as well as the influence of the right hand side of the structure ($x > 0$) have been neglected.

The configuration of a semi-infinite structure with an embedded layer in a matrix which allows for tractable analytical calculations is thus assumed to give relevant qualitative information concerning the strain threshold for the dislocation emission in the interface and its first equilibrium position. The study of the effects of the horizontal free surface of the film as well as the influence of the part of the substrate below the buckle is beyond the scope of the present analysis (Johnson and Freund, 1997; Yu et al., 2001).

The distribution of line forces introduced on the vertical free surface to model the buckle effect in the planar part of the film is derived from the stress field in its buckle part which is determined from the Föppl-von Kármán theory of thin plates. At $x = 0$, the resulting stress-tensor in a straight-sided buckle submitted to an uniaxial loading along the (Ox) axis is thus given by Hutchinson and Suo (1992) and Freund and Suresh (2003):

$$\sigma_{xx}^{FvK}(0,y) = \bar{E}_f\left[\varepsilon_c - \varepsilon_i + \left(\frac{h}{2} - y\right)\frac{\delta\pi^2}{2B^2}\right], \tag{4}$$

where ε_c is the critical strain defined in Eq. (3) beyond which the buckling occurs, ε_i is the uniaxial strain in the thin film, $\bar{E}_f = \frac{E_f}{1-\nu_f^2}$ is the Young plane modulus of the film, with E_f and ν_f the bulk Young modulus and Poisson ratio of the film respectively. The shear stresses that might be involved in the simulations are neglected in the model in order to follow the classical buckling description developed in the FvK framework. Taking these shear components of stress into account in order to improve quantitatively the predictions of the model, would imply to modify the clamped boundary

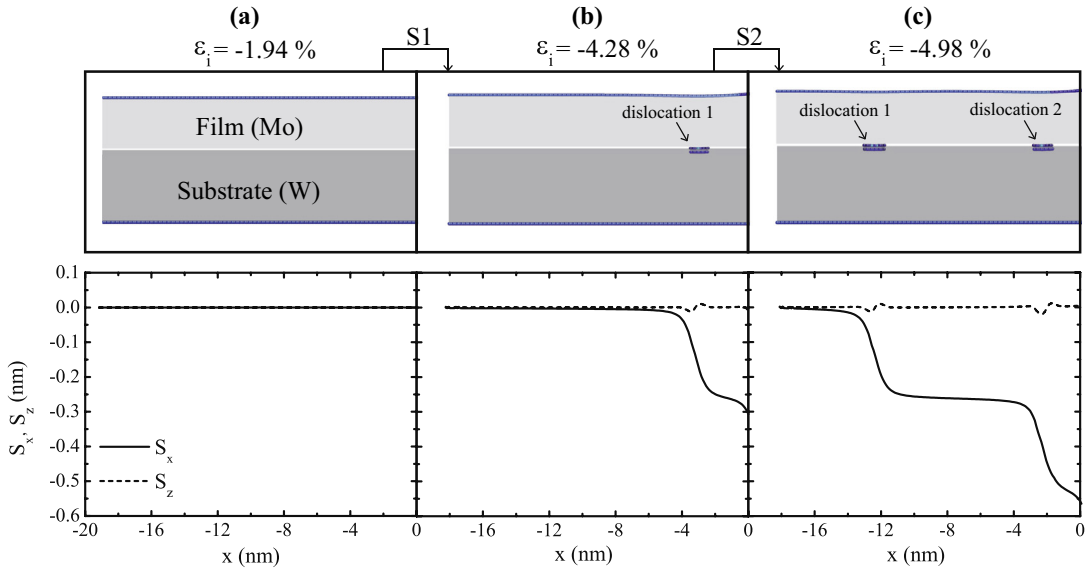

Fig. 3. (Top) Front view of the atomistic simulations of the left adherent part of the bicrystal. (Bottom) "S_x" and "S_z" components of the disregistry vector versus x.

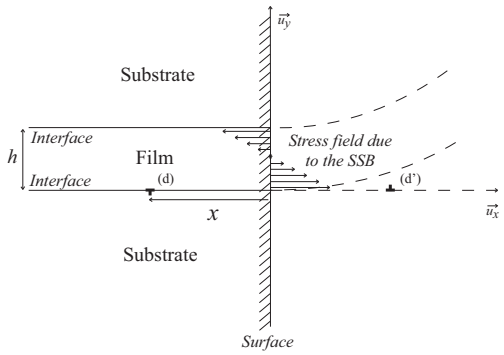

Fig. 4. Schematic of the system. A dislocation of Burgers vector $-b\vec{u_x}$ is introduced in the interface plane at a distance $x < 0$ from the surface.

conditions of the buckle considered in the FvK theory. This study is beyond the scope of the present paper.

In the case of a line force $\vec{P} = P\vec{u_x}$ whose application point is $(0,0)$, the shear component of the stress field in the half-crystal is given by Timoshenko and Goodier (1951):

$$\sigma_{xy}^{P}(x,y) = -\frac{2P}{\pi}\frac{yx^2}{(x^2+y^2)^2}, \tag{5}$$

with P scaling as a force per unit length ($N.m^{-1}$). From Eqs. (4) and (5), a force density f has been thus introduced such that $f(y) = \sigma_{xx}^{FvK}(0,y)/P$ and the shear stress component σ_{xy}^{sb} resulting from the f distribution is defined in the structure as follows:

$$\sigma_{xy}^{sb}(x,y) = \int_0^h f(y') \times \sigma_{xy}^{P}(x, y-y')\mathrm{d}y'. \tag{6}$$

From Eq. (6), the shear stress due to the buckle in the interface yields:

$$\sigma_{xy}^{sb}(x,0) = \frac{\bar{E}_f}{\pi}(\varepsilon_c - \varepsilon_i + \varepsilon_{sb})\left(\frac{h^2}{x^2+h^2}\right) + \frac{\bar{E}_f}{\pi}\varepsilon_{sb}\left(\frac{2x^2}{x^2+h^2}\right) - \frac{\bar{E}_f}{\pi}\varepsilon_{sb}\left(\frac{2x}{h}\arctan\frac{h}{x}\right), \tag{7}$$

where the strain parameter ε_{sb} is defined as:

$$\varepsilon_{sb} = \frac{h\pi}{B}\sqrt{\varepsilon_c - \varepsilon_i + \frac{\Delta}{B}}. \tag{8}$$

Another shear stress has to be taken into consideration which results from the lattice mismatch at the coherent interface between the substrate and the film. In the case where both materials have the same elastic coefficients, this shear component of the misfit stress tensor in the interface is given by Grilhé (1993):

$$\sigma_{xy}^{ep}(x,0) = -\frac{\bar{E}_f\varepsilon_{ep}}{\pi}\left(\frac{h^2}{x^2+h^2}\right), \tag{9}$$

where the misfit strain ε_{ep} accounting for the lattice mismatch is defined in Eq. (1).

Finally, once the edge dislocation is introduced, an attracting surface force has also to be considered. Following Hirth and Lothe (1982), the corresponding shear stress of the image dislocation (d′), symmetric of the interface dislocation (d) with respect to the vertical surface, writes:

$$\sigma_{xy}^{im}(x,0) = \frac{\bar{E}_f b}{8\pi x}. \tag{10}$$

It is worth noting that the expression (10) is actually the same as the expression of the image force at a crack tip derived by Rice and Thomson (1974) in the case, similar to the one of the present study, for which an edge dislocation lies in the plane of the crack with its line parallel to the crack tip.

The energy variation with respect to the strained structure free of dislocation has been thus determined. It corresponds to the work required to introduce the dislocation from $x_0 = -b$ to x in the interface, where x_0 is a cut-off length below which the elasticity theory can not be used (Hirth and Lothe, 1982). The work per unit length $\Delta W(x)$ is defined as (Grilhé, 1992):

$$\Delta W(x) = b\int_{-b}^{x}[\sigma_{xy}^{sb}(x',0) + \sigma_{xy}^{ep}(x',0) + \sigma_{xy}^{im}(x',0)]\,dx'. \tag{11}$$

The reduced expression of the energy variation $\Delta\bar{W}(\bar{x}) = \frac{\pi}{\bar{E}_f b^2}\Delta W(\bar{x})$ has been finally found to be:

$$\Delta\bar{W}(\bar{x}) = \left(\frac{\bar{b}+\bar{x}}{\bar{b}}\right)\varepsilon_{sb} - \frac{(\varepsilon_c - \varepsilon_i - \varepsilon_{ep} + \bar{b}^2\varepsilon_{sb})}{\bar{b}}\arctan\left(\frac{1}{\bar{b}}\right) - \frac{(\varepsilon_c - \varepsilon_i - \varepsilon_{ep} + \bar{x}^2\varepsilon_{sb})}{\bar{b}}\arctan\left(\frac{1}{\bar{x}}\right) + \frac{1}{8}\ln\left(\left|\frac{\bar{x}}{\bar{b}}\right|\right), \tag{12}$$

with $\bar{x} = x/h$ and $\bar{b} = b/h$.

The geometrical parameter Δ corresponding to the average slip displacement has been deduced from the simulation to be $\Delta \approx b/2$. Introducing the reduced delaminated length $\bar{B} = B/h$, the reduced energy variation $\Delta\bar{W}(\bar{x})$ has been plotted in Fig. 5 as a function of $\bar{x}$ for different values of ε_i. Taking the following set of parameters $\varepsilon_{ep} = 0.57\%, \bar{b} = b/h = 0.087$ and $\bar{B} = B/h = 6.12$ derived from the previous simulations, it is found in Fig. 5 that there exists a critical value of the uniaxial strain ε_i^* defined as $\Delta\bar{W}(\bar{x}_{eq}) = 0$ beyond which an energetically favorable equilibrium position is obtained for the dislocation at $\bar{x} = \bar{x}_{eq}$. A barrier of energy which has to be overcome to introduce the dislocation can be also deduced from the model (see Fig. 5). However in the simulations, the presence of the buckle increases the interplanar distance at the interface making the shear easier (Sun et al., 1993; Brochard et al., 2000). This mechanism is assumed to cancel the effects of the barrier of energy. It has also been found, but not shown in Fig. 5, that when the vertical surface of the structure is free from the buckle stress field, there is no equilibrium position for the dislocation at any strain ε_i. It can thus be stated at this point that the formation of the dislocation is exclusively due to the buckle, the misfit strain acting against the formation of the dislocation with a Burger vector $-b\vec{u_x}$.

The reduced equilibrium positions $\bar{x}_{eq}$ and the critical value of strain ε_i^* defined as $\Delta\bar{W}(\bar{x}_{eq}) = 0$ have been then plotted in Fig. 6 as a function of ε_i, for different values of $\bar{b}$ with $\varepsilon_{ep} = 0.57\%$. It can be underlined that for a reduced delaminated length $\bar{B} = 6.12$, the buckling occurs at $\varepsilon_i = \varepsilon_c = -2.2\%$ according to Eq. (3). At this point, it is emphasized that the main effect of the parameters ε_{ep} and $\bar{B}$ is to shift the critical strains ε_c and ε_i^*. As a

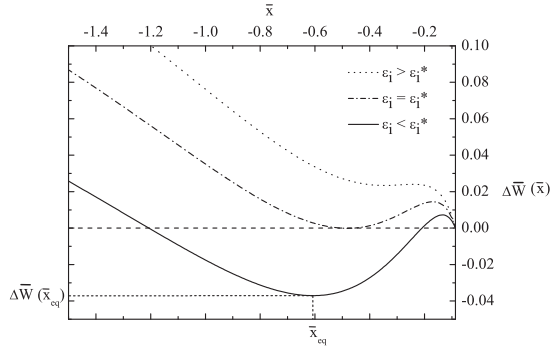

Fig. 5. Reduced energy variation $\Delta\bar{W}(\bar{x})$ as a function of $\bar{x}$, with $\varepsilon_{ep} = 0.57\%, \bar{b} = 0.087$ and $\bar{B} = 6.12$.

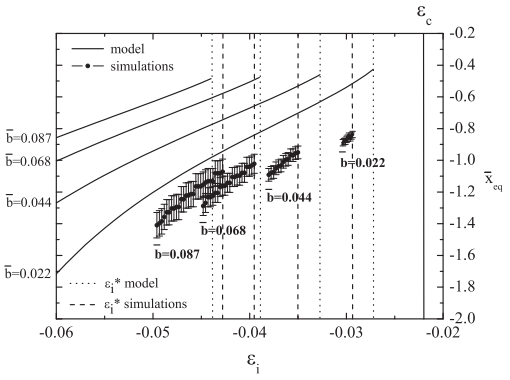

Fig. 6. Reduced equilibrium positions $\bar{x}_{eq}$ and critical strain ε_i^* derived from the model and the simulations as a function of ε_i, with $\bar{B} = 6.12$ and $\varepsilon_{ep} = 0.57\%$.

consequence, only one set of values is taken in this study for ε_{ep} and $\bar{B}$.

The equilibrium positions derived from the simulations as well as the critical strains beyond which they appear in the interface have been also displayed in Fig. 6. It is found that the values of the critical strain ε_i^*, derived from the model and the simulation, match up to ± 0.0025. The equilibrium positions determined from the model appear to be rather different from the one observed in the simulations. One possible explanation of this difference could result from the approximation of the model consisting in neglecting the effects of the horizontal free surface of the adherent part of thin film. Indeed, it can been verified in Fig. 6 that for a given Burgers vector, when the thickness h of the film increases (or $\bar{b}$ decreases), the values of the equilibrium position of the dislocation extracted from the model approaches to the ones obtained in the simulations.

The thin film evolution under increasing strain ε_i can be thus summarized as follows. For a given reduced Burgers vector $\bar{b}$, the buckling of the delaminated part of the film first occurs for $\varepsilon_i = \varepsilon_c$, the planar film/substrate interface being free of dislocation. When the strain reaches the critical value ε_i^*, a dislocation is then emitted from the buckle edge and reaches an equilibrium position corresponding to a distance from the buckle edge of the order of the thin film thickness h. Finally, a stability diagram in the $(\bar{b}, \varepsilon_i)$ plane which has been obtained from the model has been displayed in Fig. 7, the values of the critical strain extracted from the simulations being also reported. Three different regions have been identified. When the strain is low, the thin film is planar and the interface is free from any dislocation; then the film is buckled for $\varepsilon_i^* < \varepsilon_i < \varepsilon_c$ and the interface is still free from dislocation. When $\varepsilon_i < \varepsilon_i^*$, a first dislocation appears in the interface near the edge of the buckle leading to the sliding of the film on the substrate.

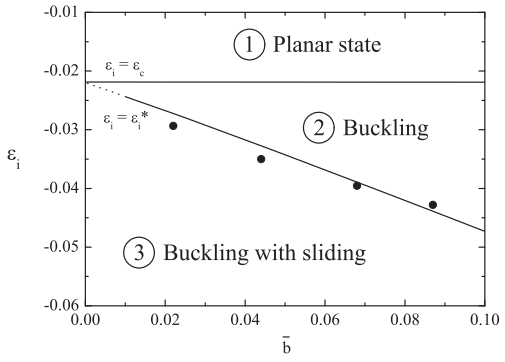

Fig. 7. Stability diagram of the film, with $\bar{B} = 6.12$ and $\varepsilon_{ep} = 0.57\%$. The black points correspond to the values of ε_i^* extracted from the simulations.

4. Conclusions

In this Paper, the formation of a dislocation in the coherent film/substrate interface after the film has buckled has been first observed from atomistic simulations. It has then been found using a simple analytical model developed in the framework of linear elasticity theory that the presence of the dislocation in the interface, near the edge of the buckle, is due to a buckle effect and the critical strain for the dislocation nucleation from the buckle edge has also been characterized. It is expected that our results should apply quantitatively to any coherent interface systems. It is believed that the fact that the introduction (or expulsion) of misfit dislocations in (or from) the adherent part is promoted when the thickness of the film increases, is a result which can be qualitatively extended to other kind of interfaces. The next step of this work would be the study of the emission of a set of dislocations from the buckle and the interaction and the subsequent evolution of these dislocations in the interface taking into account the effect of the horizontal free surface of the film.

References

Audoly, B., 1999. Stability of straight delamination blisters. Phys. Rev. Lett. 83 (20), 4124–4127.

Braun, A., Briggs, K., Böni, P., 2002. Analytical solution to Matthews and Blakeslee's critical dislocation formation thickness of epitaxially grown thin films. J. Cryst. Growth 241 (12), 231–234.

Brochard, S., Beauchamp, P., Grilhé, J., 2000. Stress concentration near a surface step and shear localization. Phys. Rev. B 61 (13), 8707–8713.

Cantu, P., Wu, F., Waltereit, P., Keller, S., Romanov, A., DenBaars, S., et al., 2005. Role of inclined threading dislocations in stress relaxation in mismatched layers. J. Appl. Phys. 97 (10), 103534.

Colin, J., Coupeau, C., Grilhé, J., 2007. Plastic folding of buckling structures. Phy. Rev. Lett. 99 (4), 046101.

Cordill, M., Moody, N., Bahr, D., 2005. The effects of plasticity on adhesion of hard films on ductile interlayers. Acta Mater. 53 (9), 2555–2562.

Cordill, M., Bahr, D., Moody, N., Gerberich, W., 2007. Adhesion measurements using telephone cord buckles. Mater. Sci. Eng. A 443 (12), 150–155.

Daw, M.S., Baskes, M.I., 1984. Embedded-atom method: derivation and application to impurities, surfaces, and other defects in metals. Phy. Rev. B 29 (12), 6443.

Demkowicz, M.J., Wang, J., Hoagland, R.G., Hirth, J., 2008. Chapter 83 interfaces between dissimilar crystalline solids. A Tribute to F.R.N. Nabarro, vol. 14. Elsevier, pp. 141–205.

Durinck, J., Coupeau, C., Colin, J., Grilhé, J., 2008. Molecular dynamics simulations of buckling-induced plasticity. Appl. Phys. Lett. 93 (22), 221904.

Durinck, J., Coupeau, C., Colin, J., Grilhé, J., 2010. A stress relaxation mechanism through buckling-induced dislocations in thin films. J. Appl. Phys. 108 (2), 026104.

Faulhaber, S., Mercer, C., Moon, M., Hutchinson, J.W., Evans, A., 2006. Buckling delamination in compressed multilayers on curved substrates with accompanying ridge cracks. J. Mech. Phys. Solids 54 (5), 1004–1028.

Frank, F., Van Der Merwe, J.H., 1949. One-Dimensional dislocations. II. misfitting monolayers and oriented overgrowth. Proc. R. Soc. Lond., Ser. A Math. Phys. Eng. Sci. 198 (1053), 216–225.

Freund, L.B., Suresh, S., 2003. Thin Film Materials-Stress, Defects Formation and Surface Evolution. Cambridge University Press, Cambridge.

Gao, H., 1994. Some general properties of stress-driven surface evolution in a heteroepitaxial thin film structure. J. Mech. Phys. Solids 42 (5), 741.

Gioia, G., Ortiz, M., Hutchinson, J.W., Wu, T.Y., 1997. Delamination of Compressed Thin Films. Elsevier, pp. 119–192.

Godet, J., Brochard, S., Pizzagalli, L., Beauchamp, P., Soler, J.M., 2006. Dislocation formation from a surface step in semiconductors: an ab initio study. Phys. Rev. B 73 (9), 092105.

Grilhé J., Junqua N. 1992. Stress calculations in thin films and multilayers using distributions of infinitesimal dislocations. In: MRS Proc. 239, pp. 527.

Grilhé, J., 1993. Mechanical properties of layered structures and thin films on substrates. In: Nastasi, M., Parker, D.M., Gleiter, H. (Eds.), Mechanical properties and deformation behavior of materials having ultra-fine microstructures, NATO-ASI Series E: Applied Sciences. kluwer, dordrecht, p. 255.

Henager, C.H., Hoagland, R.G., 2004. A rebound mechanism for misfit dislocation creation in metallic nanolayers. Scripta Mater. 50 (5), 701–705.

Hirth, J., Lothe, J., 1982. Theory of Dislocations. John wiley and sons.

Hu, M., Evans, A., 1989. The cracking and decohesion of thin films on ductile substrates. Acta Metall. 37 (3), 917–925.

Hutchinson, J.W., Suo, Z., 1992. Mixed mode cracking in layered materials. Adv. Appl. Mech. 29 (63–191).

Johnson, R.A., 1989. Alloy models with the embedded-atom method. Phys. Rev. B 39 (17), 12554.

Johnson, H.T., Freund, L.B., 1997. Mechanics of coherent and dislocated island morphologies in strained epitaxial material systems. J. Appl. Phys. 81 (9), 6081–6090.
Kuznetsov, A.S., Gleeson, M.A., Bijkerk, F., 2012. Hydrogen-induced blistering mechanisms in thin film coatings. J. Phys. Condens. Matter. 24 (5), 052203.
Lee, A., Litteken, C., Dauskardt, R., Nix, W., 2005. Comparison of the telephone cord delamination method for measuring interfacial adhesion with the four-point bending method. Acta Mater. 53 (3), 609–616.
Matthews, J., Blakeslee, A., 1974. Defects in epitaxial multilayers: I. misfit dislocations. J. Cryst. Growth 27, 118–125.
Parry, G., Coupeau, C., Colin, J., Cimetière, A., Grilhé, J., 2004. Buckling and post-buckling of stressed straight-sided wrinkles: experimental AFM observations of bubbles formation and finite element simulations. Acta Mater. 52 (13), 3959–3966.
Plimpton, S., 1995. Fast parallel algoritms for short-range molecular dynamics. J. Comput. Phys. 117, 1–19.
Rice, J.R., Thomson, R., 1974. Ductile versus brittle behaviour of crystals. Phil. Mag. 29 (1), 73–97.
Ruffini, A., Durinck, J., Colin, J., Coupeau, C., Grilhé, J., 2012. Gliding at interface during thin film buckling: a coupled atomistic/elastic approach. Acta Mater. 60 (3), 1259–1267.
Shao, S., Medyanik, S.N., 2010. Dislocation-interface interaction in nanoscale fcc metallic bilayers. Mech. Res. Commun. 37 (3), 315–319.
Spearot, D., Jacob, K., McDowell, D., 2007. Dislocation nucleation from bicrystal interfaces with dissociated structure. Int. J. Plast. 23 (1), 143–160.
Sun, Y., Beltz, G.E., Rice, J.R., 1993. Estimates from atomic models of tension-shear coupling in dislocation nucleation from a crack tip. Mater. Sci. Eng.: A 170 (1–2), 67–85.
Timoshenko, S.P., Goodier, J.N., 1951. Theory of Elasticity, third ed., 1, Mc-Graw-Hill International.
Yang, F., 2006. Stress-induced surface instability of an elastic layer. Mech. Mater. 38 (12), 111–118.
Youssef, S., Neily, S., Gutakowskii, A.K., Bonnet, R., 2008. Dislocation bends in a film/substrate heterostructure. Scripta Mater. 58 (1), 1–4.
Yu, H., He, M., Hutchinson, J.W., 2001. Edge effects in thin film delamination. Acta Mater. 49 (1), 93–107 (951).
Zhao, M., Fu, R., Lu, D., Zhang, T., 2002. Critical thickness for cracking of Pb(Zr0.53Ti0.47)O3 thin films deposited on Pt/Ti/Si(100) substrates. Acta Mater. 50 (17), 4241–4254.
Zhou, X.W., Wadley, H.N.G., Johnson, R.A., Larson, D.J., Tabat, N., Cerezo, A., et al., 2001. Atomic scale structure of sputtered metal multilayers. Acta Mater. 49 (19), 4005–4015.